Cohesin mediated loop extrusion from active enhancers form chromatin jets in *C. elegans*

Jun Kim[1], Sevinç Ercan[1#]

[1] Department of Biology, Center for Genomics and Systems Biology, New York University, New York, NY, USA

[#] corresponding author
email: sevinc@nyu.edu

Abstract

In mammals, cohesin and CTCF organize the 3D genome into topologically associated domains (TADs) to regulate communication between cis-regulatory elements. However, many organisms, including *S. cerevisiae*, *C. elegans*, and *A. thaliana* lack CTCF. Here, we use *C. elegans* as a model to investigate the function of cohesin in 3D genome organization in an animal without CTCF. We use auxin-inducible degradation to acutely deplete SMC-3 or its negative regulator WAPL-1 from somatic cells. Using Hi-C data, we identify a cohesin-dependent 3D genome feature termed chromatin jets (aka fountains), also observed in zebrafish and mammalian genomes. The jets emerge from NIPBL occupied segments, and the trajectory of the jets coincides with cohesin binding. The spreading of cohesin from jet origins depends on a fully intact cohesin complex and is extended upon WAPL-1 depletion. These results support the idea that cohesin is preferentially loaded at NIPBL occupied sites, from which cohesin loop extrudes in an effectively two-sided manner. The location of putative loading sites coincides with active enhancers and the pattern of chromatin jets correlates with transcription. We propose that in the absence of CTCF, preferential loading of cohesin at enhancers is a conserved mechanism of genome organization that regulates the interaction of gene regulatory elements in 3D.

Introduction

In mammalian genomes, cohesin and CTCF form topologically associating domains (TADs) (1). The current model of TAD formation encompasses three main features: 1) cohesin is uniformly loaded, 2) cohesin performs two-sided loop extrusion, and 3) loop extrusion is stalled at CTCF-binding sites located at TAD boundaries (2). The second and the third assumptions of the model are visualized *in vitro* using single-molecule assays, thus bridging the gap between the theoretical model and the experimental observation *in vivo* (3, 4).

The first assumption of the model, uniform loading of cohesin, is less well supported *in vivo*. Recent studies suggest that cohesin may be preferentially loaded at specific sites, leading to the

formation of Hi-C detected features termed “jets”, “plumes” or “fountains” depicted as secondary diagonals protruding from narrow segments (5-9). The preferential loading sites locally increase the frequency of cohesin loops, thus providing another layer of 3D genome folding, which is shorter in scale compared to TADs. Such a mechanism of genome folding could have strong regulatory implications for species lacking CTCF.

Caenorhabditis elegans is a small animal with a ~100 Mb genome and no CTCF (10). In the mammalian system, the cohesin is composed of four subunits, SMC1, SMC3, RAD21, and STAG (11). The STAG subunit has two isoforms STAG1 and STAG2 that forms cohesin in mutually exclusive manner (12). In *C. elegans*, the three of the four subunits of cohesin, SMC-1, SMC-3, and SCC-3 (STAG), has a single copy, while the kleisin subunit has 5 variants: COH-1, COH-2 (aka SCC-1), COH-3, COH-4, and REC-8 (13, 14). COH-2, but not COH-1, has mitotic functions, while COH-3/4 (paralogs) and REC-8 have meiotic functions (15-18).

In this study, we applied auxin-inducible degradation to acutely deplete SMC-3 or its negative regulator WAPL-1 from somatic cells in *C. elegans* early-L3 larvae with 1 hour auxin treatment. We performed Hi-C analyses in control, SMC-3 and WAPL-1 depletion conditions, and identified over 250 cohesin-dependent chromatin jets. Upon depletion of SMC-3 or WAPL-1, the jets are lost or extended, respectively. The jets emerge from the cohesin loader NIPBL occupied segments that overlap with active enhancers but not promoters, and the trajectory of the jets coincides with the spreading of cohesin. Prominent chromatin jets are observed over clusters of actively transcribed genes. One hour depletion of cohesin does not affect the binding of RNA Polymerase II and NIPBL. Together, our results suggest that cohesin is preferentially loaded at NIPBL occupied active enhancers, from which cohesin loop extrudes bi-directionally forming chromatin jets.

Materials and Methods

Worm strain and growth

Worms were grown and maintained at 20-22°C on Nematode Growth Medium (NGM) plates containing *E. coli* strains OP50-1 and/or HB101. To isolate synchronized L2/L3 worms, gravid adults were bleached in 0.5 M NaOH and 1.2% bleach, and embryos were hatched overnight in M9 buffer (22 mM KH2PO4 monobasic, 42.3 mM Na2HPO4, 85.6 mM NaCl, 1mM MgSO4). The resulting starved L1s were grown for 24 hours at 22°C. Degron-GFP tagged alleles were produced by SUNY Biotech and crossed to CA1200 strain expressing TIR1 under the control of eft-3 promoter to produce ERC102 syb5520 [smc-3::GGGGS::AID::emGFP] III , [eft-3p::TIR1::mRuby::unc-54 3'UTR + Cbr-unc-119(+)] II and ERC103 syb6035 [wapl-1::GGGGS::AID::emGFP] IV, [eft-3p::TIR1::mRuby::unc-54 3'UTR + Cbr-unc-119(+)] II.

Auxin treatment

Auxin (indole-3-acetic-acid, Fisher 87-51-4) was resuspended in 100% ethanol to a concentration of 400 mM. Plates were prepared by adding resuspended auxin at a concentration of 1 mMto NGM media before pouring. Synchronized L2/L3 worms were washed three times with M9 and split into two. Half of the worms were transferred to NGM 10 cm plates containing 1mM of auxin. The other half were placed in normal NGM 10 cm plates (no-auxin control). A

maximum of 300µL of settled worms was placed in one 10 cm plate. Worms were then washed one time with M9 and processed according to future application. For ChIP and Hi-C, worms were crosslinked in 2% formaldehyde for 30 minutes, followed by quenching in 125mM glycine for 5 minutes, one wash with M9 and two washes with PBS, PMSF and protease inhibitors. For RNA-seq, worms were stored in Trizol.

ChIP-seq

Two biological replicates with matching input samples were performed for each experiment. Around 100 µL of L2/L3 larvae were dounce-homogenized with 30 strokes in FA buffer (50 mM HEPES/KOH pH 7.5, 1 mM EDTA, 1% Triton X-100, 0.1% sodium deoxycholate, 150 mM NaCl) supplemented with PMSF and protease inhibitors (Calbiochem, 539131). Dounced worms were sonicated in 0.1% sarkosyl or 15 minutes using a Picoruptor to obtain chromatin fragments between 200 and 800 bp. Protein concentration was determined using Bradford assay (Biorad 500-0006). 1-2 mg of protein extract was used per ChIP and 5% was taken out to use as input DNA. The remaining protein extract was incubated with 3 to 10 ug of antibody at 4°C rotating overnight in a volume of 440µL. 40µL of (1:1V) Protein A and/or G Sepharose beads that were previously washed 3 times with FA buffer, were added and incubated, rotating at 4°C for 2 hours. Beads were washed with 1mL of each of the following buffers: 2 times with FA buffer, 1 time with FA-1mM NaCl buffer, 1 time with FA-500mM NaCl buffer, 1 time with TEL buffer (0.25 M LiCl, 1% NP-40, 1% sodium deoxycholate, 1 mM EDTA, 10 mM Tris-HCl, pH 8.0) and 2 times with TE buffer. Immunoprecipitated chromatin was eluted from beads by incubating in ChIP elution buffer (1% SDS, 250 mM NaCl, 10 mM Tris pH 8.0, 1 mM EDTA) at 65°C for 30 minutes, treated with Proteinase K and reverse crosslinked at 65°C overnight. Half of the ChIP DNA and 30 ng of input DNA were used for library preparation. End repair was performed in T4 ligase reaction buffer (New England Biolabs, NEB), 0.4mM of dNTPs, 20 U of T4 Polynucleotide kinase (NEB), 3.5 U of Large (Klenow) fragment (NEB) and 6 U of T4 DNA polymerase for 30 minutes at 20°C in a total volume of 33 µL. Reaction was cleaned using Qiagen MinElute PCR purification kit. A-tailing reaction was performed in NEB buffer 2, 0.2 mM of dATPs and 7.5 U of Klenow fragment-exo (NEB) at 37°C for 60 minutes in 25 µL. Reaction was cleaned using Qiagen MinElute PCR purification kit. Illumina TruSeq adapters were ligated to DNA fragments in a reaction containing 2X Quick ligation buffer (NEB), 0.25 µM of adapter and 2 µL of Quick ligase (NEB) for 20 minutes at 23°C in 40 µL. Reaction was cleaned using Agencourt AMPure XP beads and the eluted DNA was PCR amplified in 50 µL using Phusion Polymerase and TruSeq primers, forward: AAT GAT ACG GCG ACC ACC GAG ATC TAC ACT CTT TCC CTA CAC G*A, reverse: CAA GCA GAA GAC GGC ATA CGA GA*T, where * represents a phosphorothioate bond. PCR reactions were cleaned using Qiagen MinElute PCR purification kit. The eluted DNA was run on a 1.5% agarose gel and fragments between 250-600 bp were gel extracted using Qiagen gel extraction kit. Library concentration was determined using KAPA Library quantification kit. Single-end 75 bp sequencing was performed using the Illumina NextSeq 500.

Hi-C

Two biological replicates were performed for each experiment. Crosslinked L2/L3 worms collected as described above were resuspended in 20 ul of PBS per 50ul of worm pellet, then dripped into liquid nitrogen containing mortar. The worms were grounded with pestle until fine powder. Grounded worms were crosslinked again in 2% formaldehyde using the TC buffer as

described by the Arima High Coverage Hi-C kit, which uses four 4-base cutters, DpnII, HinfI, DdeI, and MseI. The Arima manufacturer's protocol was followed including the recommended method of the library preparation using KAPA Hyper Prep Kit. Paired-end 100 bp sequencing was performed using the Illumina Novaseq 6000 at the New York University Center for Genomics and Systems Biology, New York, NY.

Microscopy
The worms were washed off the plate in M9 buffer, crosslinked in 0.5% formaldehyde for 15 minutes and 'freeze cracked' by submerging in liquid nitrogen for 1 minute and then thawing in 37°C water bath. The worms were washed twice using 70% ethanol followed by a third wash using the wash buffer (PBS-0.05% Tween-20). The worms were resuspended in 1mL of wash buffer and 1ul of 2ug/mL DAPI (FisherEN62248) and were incubated in 37°C water bath for 30 minutes. The worms were then washed twice in PBS and imaged on slides for DAPI and GFP.

ChIP-seq data processing and analysis
Bowtie2 version 2.4.2 was used to align 75 bp single-end reads to WS220 with default parameters (19). Bam sorting and indexing was performed using samtools version 1.11 (20). BamCompare tool in Deeptools version 3.5.0 was used to normalize for the sequencing depth using CPM and create ChIP-Input coverage with a bin size of 10 bp and 200 bp read extension (21). Only reads with a minimum mapping quality of 20 were used, and mitochondrial DNA, PCR duplicates, and blacklisted regions were removed (22). The average coverage data was generated by averaging ChIP-Input enrichment scores per 10 bp bins across the genome.

Hi-C data processing and analysis
Hi-C data analysis: The Hi-C data was mapped to ce10 (WS220) reference genome using default parameters of the Juicer pipeline version 1.5.7 (23). The biological replicates were combined using juicer's mega.sh script. The mapping statistics from the inter_30.txt output file are provided. The inter_30.hic outputs were converted to cool format using the hicConvertFormat of HiCExplorer version 3.6 (24, 25) in two steps using the following parameters: 1) --inputFormat hic, --outputFormat cool, 2) --inputFormat cool --outputFormat cool --load_raw_values. The cool file was balanced using cooler version 0.8.11 using the parameters: --max-iters 500, --mad-max 5, --ignore-diags 2 (26). The balanced cool file was used for all downstream analysis.
For computing log-binned P(s) and its log-derivative cooltools version 0.4.0 (https://github.com/open2c/cooltools) was used. For visualizing ChIP-seq data with Hi-C data in python, pyBigwig version 0.3.18 (https://github.com/deeptools/pyBigWig) was used.

Sequencing data and analysis script availability
The data are available at the Gene Expression Omnibus under GSE237663. A list of data and statistics are provided in Supplemental File 1. Analysis scripts are provided at https://github.com/ercanlab/2023_Kim_cohesin.

Results

Acute depletion of cohesin and WAPL from somatic cells

In *C. elegans*, there is a singular subunit for SMC-1, SMC-3, and SCC-3 (Figure 1A) (16). To

study the effect of cohesin loss, we targeted SMC-3 subunit for auxin inducible degradation. In conjunction, to study the enhanced activity of cohesin, we targeted WAPL (encoded by gene named *wapl-1* in *C. elegans*), a negative regulator of cohesin (27, 28). The *C. elegans* ortholog of the cohesin loader NIPBL is encoded by the gene *pqn-85*/*scc-2* (29). The two proteins, SMC-3 and WAPL were C-terminally tagged with degron-gfp at the endogenous locus using strategies employed previously (30, 31). To analyze somatic cells, we used worms in the early L3 stage, at which point most somatic cells have stopped dividing and the germline has not started proliferating (32). To knock down cohesin specifically in the somatic cells, we used the background strain in which the auxin response gene TIR1 is under the control of a soma-specific promoter *eft-3* (30, 31). This background strain is used as a control where TIR1 is expressed but none of the endogenous genes are tagged with degron-gfp (Figure 1B).

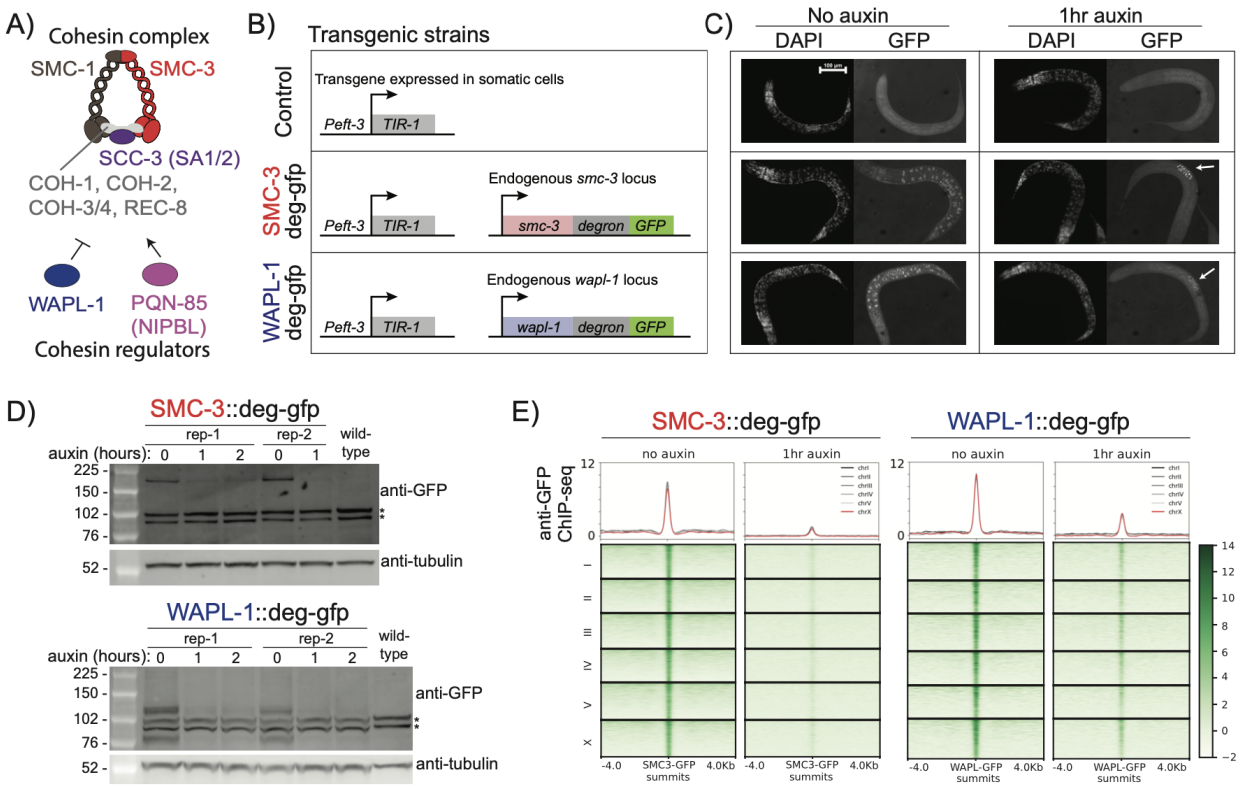

Figure 1. Acute depletion of cohesin and WAPL from somatic cells.
A) *C. elegans* subunits of cohesin and its regulators. B) Transgenic strains used in this paper. Exogenously inserted TIR1 is expressed in somatic cells using the *eft-3* promoter. Endogenous *smc-3* or *wapl-1* are C-terminally tagged with degron-gfp. C) DAPI and GFP images of L3 stage worms. White arrow indicates that the proteins in the germline are not degraded upon auxin treatment due to TIR1 presence only in the somatic cells. Scalebar: 100um. D) Western blot images of L3 stage worms with increasing auxin treatment duration. Anti-GFP antibody was used to show global depletion of the tagged protein. Anti-tubulin antibody was used as loading control. Asterisk indicates background bands. E) Meta-plot of ChIP-seq data grouped into different chromosomes. Anti-GFP antibody was used to show uniform depletion of SMC-3 and WAPL.

Upon visualizing DAPI and GFP, we observe that in the control condition, both cohesin and WAPL show ubiquitous GFP signals, suggesting that cohesin and WAPL are present in the all interphase as well as the few germ cells present in early L3 larvae (Figure 1C, no auxin). Upon auxin treatment, both cohesin and WAPL are noticeably depleted in somatic cells but are maintained in the germline as expected from somatic expression of TIR1 (Figure 1C, 1hr auxin). At population average, western blot analysis of degron-GFP tagged proteins show noticeable depletion in the total amount of protein (Figure 1D). This depletion is maximally achieved by 1-hour treatment, and no further depletion was observed upon 2-hour treatment. Therefore, we chose 1-hour as a general 'depletion condition' to minimize the potential indirect effect. Lastly, we performed ChIP-seq using anti-GFP antibodies and observed uniform depletion across the genome (Figure 1E). In summary, both SMC-3 and WAPL are acutely depleted from somatic cells with 1-hour auxin treatment.

WAPL depletion increases cohesin binding away from NIBPL sites

In vitro, SMC complexes translocate along DNA [12, 37-39]. *In vivo*, this dynamic process manifests in ChIP-seq signal track as 'spreading', where the enrichment gradually decreases with increasing genomic distance from a loading source (33). In bacteria, insertion of *parS* sequences result in spreading of bacterial SMC complex (34-36). In worms, an X-specific condensin spreads out from its recruitment elements on the X (30, 37, 38). Recently, targeted loading of cohesin using tetO-tetR system also showed spreading of cohesin binding at nearby CTCF sites (39). Thus, observation of spreading implies the presence of loading sites.

In the control condition, we observe that cohesin binding shows a mix of peaks and background enrichment of ChIP-seq signal, creating cohesin bound-domains (Figure 2A, black panel). These domains are of different sizes and coincide with active genes (Figure2B). Importantly, the distance of cohesin binding is extended upon depletion of WAPL, suggesting cohesin spreads further from loading sites (Figure 2A, blue panel). Given that WAPL functions to suppress the residence time of cohesin on DNA, we conclude that the observed spreading reflects a dynamic process, whereby the distance traveled depends on the time cohesin resides on the DNA.

Cohesin spreads out from NIPBL occupied sites

Upon SMC-3 depletion, residual amounts of SMC-1 can be detected in the middle of the spreading region (Figure 2A, red panel). Given that cohesin requires ATP hydrolysis to translocate *in vitro* (4), and that ATP hydrolysis requires heterodimerization of head subunits from both SMC-1 and SMC-3 (40, 41), we speculate that the residual SMC-1 signal reflects the initial loading site for cohesin. We test this idea by performing ChIP-seq for cohesin loader NIPBL (also known as SCC-2 or PQN-85 in *C. elegans*) in the control condition. ChIP-seq signal for NIPBL does not track cohesin spreading and resembles the binding pattern of the residual SMC-1 in SMC-3 depletion (Figure 2A). While whether NIPBL is a loader and processivity factor is still debated (39, 42-45), the lack of spreading pattern in NIPBL track suggests that NIPBL functions as a loader rather than a processivity factor that moves with cohesin in *C. elegans*.

We further analyzed the shift in cohesin binding from control to WAPL depletion conditions. Upon WAPL depletion, cohesin binding is reduced within the control cohesin binding domains, while increasing outside (Figure 2A, B). Genome-wide, the number of cohesin binding sites

(inferred from SMC-1 and SMC-3 peaks) are comparable, but distinct between control and WAPL depletion conditions (Figure 2C). Furthermore, the peaks that appear upon WAPL depletion are further from the nearest NIPBL binding sites (Figure 2D). Together, these results suggest that cohesin travels away from NIPBL sites with increasing residence time and support a model in which cohesin is initially loaded at a putative loading site occupied by NIPBL, from which cohesin spreads dynamically in bi-directional fashion.

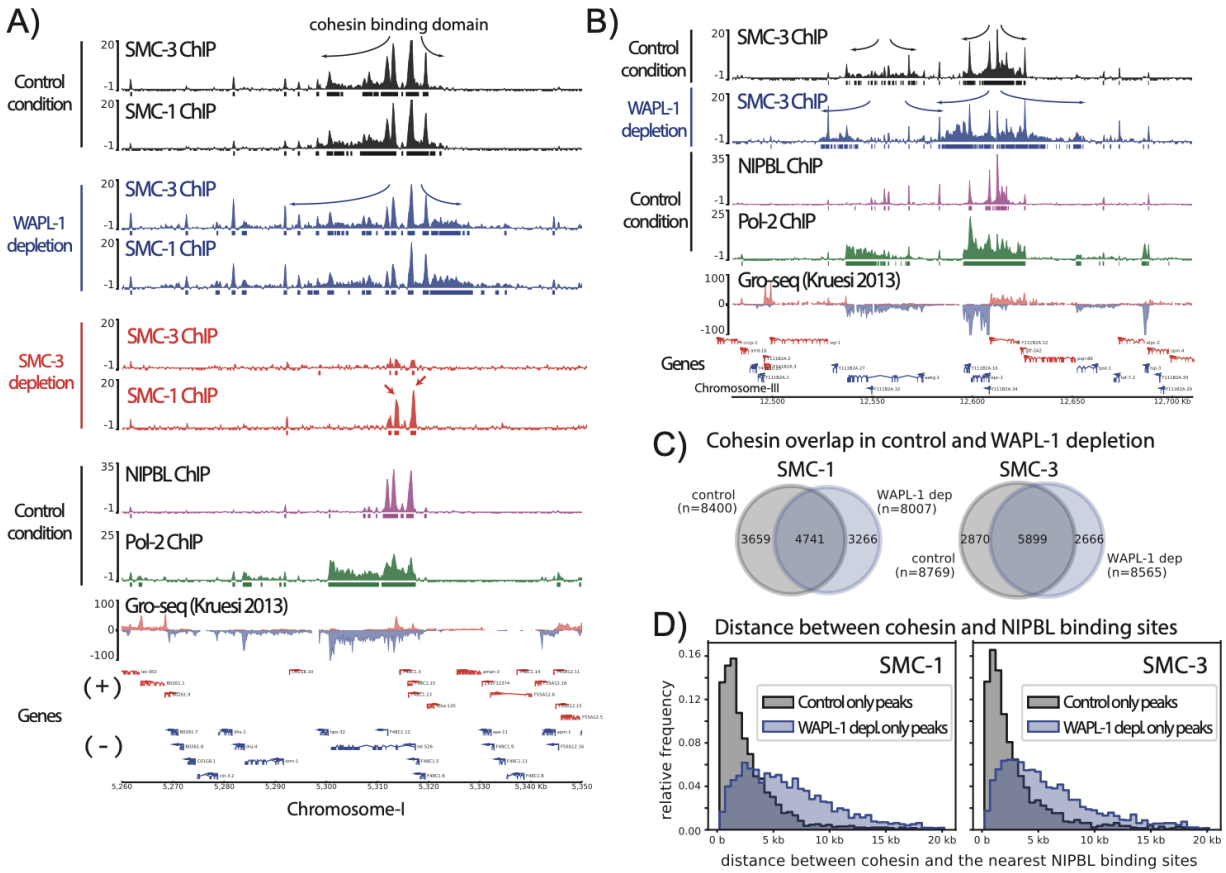

Figure 2. Cohesin spreads bi-directionally from putative loading sites.
A) Genome browser view of a cohesin enriched domain. Shown are cohesin binding (SMC-3 and SMC-1) in control condition (top black panel), WAPL depletion condition (blue panel), and SMC-3 depletion condition (red panel). NIPBL, RNA Pol II and GRO-seq (46) in control condition are shown below (bottom black panel). B) A second example illustrates two domains. One more diffuse with shorter and distributed NIBPL peaks (left) and the other with more focal and strong NIBPL peaks (right). C) Venn diagram showing difference in cohesin binding sites inferred from MACS2 narrow peak-caller in control vs. WAPL depletion conditions. D) Relative frequency of distance between cohesin peaks to the nearest NIPBL binding sites. Only the control or WAPL depletion specific peaks were used to illustrate the increased distance of peaks in WAPL condition.

Bi-directional spreading of cohesin forms chromatin jets detected by Hi-C

In vitro, cohesin performs two-sided loop extrusion (3, 4). In simulation, cohesin was inferred to be an *effectively* two-sided loop extruding factor based on Hi-C data (47). *In vivo*, recent

observation of chromatin jets or plumes further supports cohesin as a two-sided loop extruding factor (5-9). DNA-damage induced recruitment of cohesin or artificial loading of cohesin via a tetO-tetR system generated 'stripe', suggesting that cohesin could also act as a one-sided loop extruding factor (39, 48). Our population average ChIP-seq data (Figure 2) cannot distinguish whether the spreading of cohesin towards left and right occur simultaneously, which would imply two-sided loop extrusion, or independently, which would imply one-sided loop extrusion. Thus, we performed Hi-C to distinguish between the two different underlying behaviors of cohesin.

In the control condition, we observe a short chromatin jet (Figure 3A, left) at the example region presented in Figure 2A. In the SMC-3 depletion, the jet is lost, indicating that the jet is cohesin dependent (Figure 3A, center). In the WAPL depletion condition, where cohesin spreads farther, the jet is extended, suggesting that cohesin initially forms a smaller loop and then a larger loop with increasing residence time on DNA (Figure 3A, right). Consistent with ChIP-seq data showing that cohesin spreads farther towards left than right (Figure 2A), the jet shows left-ward tilt (Figure 3). Our Hi-C data suggests that loop extrusion by cohesin is effectively two-sided.

Chromatin jet origins coincide with strong NIPBL binding

ChIP-seq analysis of cohesin binding and the resulting chromatin jets suggest that cohesin is preferentially loaded at the jet origins. We define jets as a segment of DNA that have locally enriched contacts near the main diagonal that reduces upon cohesin depletion and shows a peak in control and WAPL depletion (Figure 3 Supplement 1). The 'jet strength' is calculated from the peak prominence of insulation score from control-cohesin conditions, thus measuring cohesin dependence. Meta analysis of average Hi-C signal in quartiles of jet strength confirmed the identification of cohesin dependent chromatin jet origins (Figure 3B).

If jets are formed by focal loading of cohesin by NIPBL, jet origins and strength should correlate with NIPBL binding. Indeed, the strength of the jet positively correlated with both average NIPBL ChIP-seq signal (Figure 3C) as well as the number of NIPBL peaks (Figure 3D).

Next, we considered the alternative idea that rather than preferential loading at NIBPL sites, the observed cohesin binding is a reflection of stalling. In the bacterial and mammalian systems, RNA polymerase II functions as a moving barrier for loop extrusion (33, 43). In the control condition, cohesin signal coincides with published GRO-seq and RNA Pol II ChIP-seq data (Figure 2A). However, two Hi-C features that were reported to reflect the barrier effect of RNA Pol II were not detected in our data. We observe 1) no broad 'stripe' originating from the transcribed gene body that would be predicted if cohesin is stalled by broadly distributed RNA Pol II along the gene body, and 2) no insulation effect across the gene body as cohesin fails to facilitate contacts across. Instead, interaction across the cohesin spreading region is facilitated, not insulated. Combined with the observations that chromatin jet strength correlates with focal NIPBL binding, we conclude that cohesin enrichment at jets is a reflection of increased loading rather than stalling.

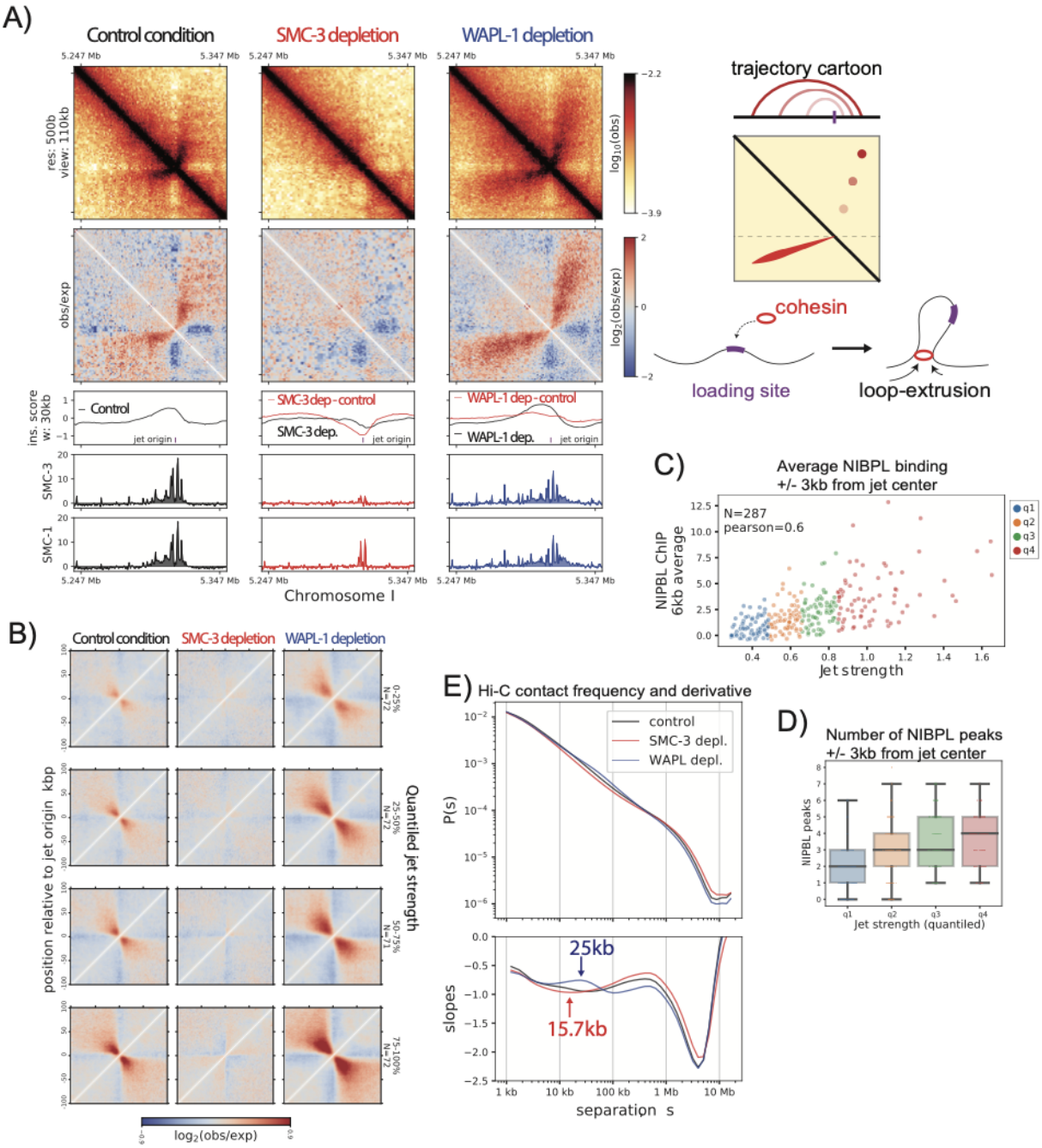

Figure 3. Bi-directional spreading of cohesin forms chromatin jets
A) Hi-C snapshot of the cohesin binding domain shown in Figure 2A in control, SMC-3 and WAPL depletion conditions. Going from the top to bottom row: The observed balanced matrix, distance-decay normalized observed-over-expected matrix, insulation score using 30kb-window and 500bp-step (black lines – condition (control of depletions), red lines – condition minus the control), and cohesin ChIP-seq data are plotted. Both Hi-C and ChIP-seq data are binned over 500bp. The jet origins inferred from Hi-C data are marked as purple vertical ticks with insulation scores. Total of 287 jets are identified using Hi-C data. B) On-diagonal pileup of observed-over-expected matrix centered at jet origins quantiled based on the jet strength for three conditions. C) Scatter plot of jet strength vs. NIPBL ChIP average

signal over 6kb region in control condition. The jet strength corresponds to peak prominence in the Hi-C insulation score change upon cohesin knockdown (control minus SMC-3 depletion). D) Boxplot of jet strength (divided into four equal groups) and the number of called NIPBL peaks. E) Contact probability, P(s), as a function of linear genomic separation between pairs of loci, s (top row), and its log-derivative, the slopes of P(s) in log-space, (bottom row) are plotted for three conditions in different colors. The inferred average loop size for cohesin in unperturbed state (red arrow) and the extended average loop size for cohesin in WAPL depletion condition (blue arrow) are annotated. Only data from autosomes were used.

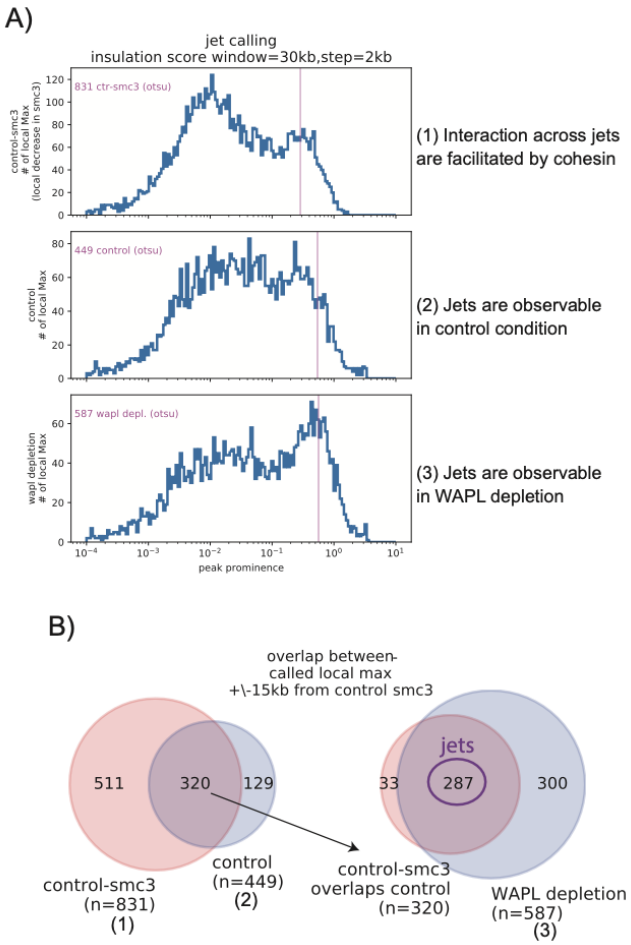

Figure 3 – Supplement 1. Jet calling method

A) Histogram of local maxima with varying degree of peak prominence. We reason that identified 'jets' must be (1) facilitated by cohesin, (2) observable in control condition, and (3) observable in WAPL condition. These three conceptual criteria are applied computationally as identifying significant local maxima of (1) insulation scores delta (control condition minus SMC3 depletion condition), (2) insulation scores in control condition, and (3) insulation scores in WAPL depletion condition. The 'jet strength' in Figure 3C,D is the peak prominence of insulation scores delta (1), ie. the strength of interaction facilitated by cohesin. The significant local maxima are called based on Otsu's method of signal-noise separation. B) Pair-wise overlap between significant local maxima called from above criteria. Due to shift in the maxima occurring from tilt of the jets, the 'overlap' allows for +/-15kb maximum distance

(half of the insulation score window) from the local maxima called by insulation delta (1). We reason that insulation delta (1) provides the most accurate position and strength of the jet origin since it corrects for underlying Hi-C structure that is not cohesin dependent.

Cohesin-mediated DNA loops in C. elegans are shorter than those observed in mammals

While the jets are pronounced Hi-C features, they may reflect above-average cohesin behaviors on chromatin. The contact probability curve, P(s), and its log-derivative are powerful metrics for estimating the average loop size of the chromosome (49, 50). In the mammalian system, cohesin forms 100-200 kb loops on average (3, 50), while the jets can propagate up to 1 to 2 Mb (6). Here, we use the similar metric to infer cohesin loop size. We excluded the X chromosomes due to the activity of a dosage compensation-specific condensin (38). While we do not observe a local maximum in the log-derivative of P(s) that disappears in the SMC-3 depletion condition, we observe a more pronounced local minima in the SMC-3 depletion condition. We use this to infer that cohesin makes loops of size 15.7 kb (Figure 3E, red arrows). In the WAPL depletion, a local maximum is readily observed, indicating that cohesin makes more extended loops of size 25 kb (Figure 3E, blue arrows). These numbers are smaller than the length of exemplary jets, which can extend up to ~50kb (Figure 3). We conclude that average *C. elegans* cohesin loops are ~10 fold smaller than the ones formed by the mammalian cohesin and chromatin jets may be formed by cohesin molecules with higher-than-average processivity.

Chromatin jet patterns are influenced by loading and clashing of cohesin molecules

Analyses of Hi-C patterns upon WAPL depletion suggest that loading and clashing of cohesin complexes determine the structure and trajectory of the chromatin jets. Broad loading of cohesin was proposed to create domains of increased 3D contacts with extension from the diagonal (6). Indeed, we observed that at a cohesin binding domain with broad NIPBL binding, the diagonal Hi-C interactions were further extended upon WAPL depletion, supporting that this particular chromatin jet is formed by cohesin molecules loaded over a broad region (Figure 4A, B).

In the genomic region with two cohesin binding domains (Figure 2B), Hi-C analysis upon WAPL depletion suggests clashing of cohesin molecules (Figure 4C). The cohesin domain on the left is marked by lower cohesin ChIP-seq signal and small but numerous NIPBL peaks (Figure 4D). The domain on the right is marked by stronger and more focal NIPBL binding. Upon WAPL depletion, the resulting Hi-C pattern suggests that the cohesin molecules originating from the two domains stall in the middle, while continually extruding on the opposing sides (Figure 4C). This creates diffuse stripes emanating from the putative sites of stalling and increases contacts between the two loop domains further away from the main diagonal.

In summary, the loading of cohesin at jet origins occur at a high frequency such that the two cohesins loaded at two closely located genomic locations often run into each other resulting in a domain-like structure if the loading sites are broad/clustered (Figure 4A), or in a jet-to-stripe transition if the two loading sites are separated by a short distance (Figure 4C).

Chromatin jet origins coincide with accessible active enhancers

Cohesin mediated chromatin jet origins overlapped with several proteins and histone marks associated with active enhancers but not promoters (Figure 4B, C). To analyze this overlap

genome-wide, we compared the jet origins to genome annotations from two previous studies (51, 52). Genomic regions designated as active enhancers by Daugherty et al. were closer to jet origins compared to other annotations (Figure 4D). Evans et al. split active enhancers into intergenic and intragenic (Figure 4E).

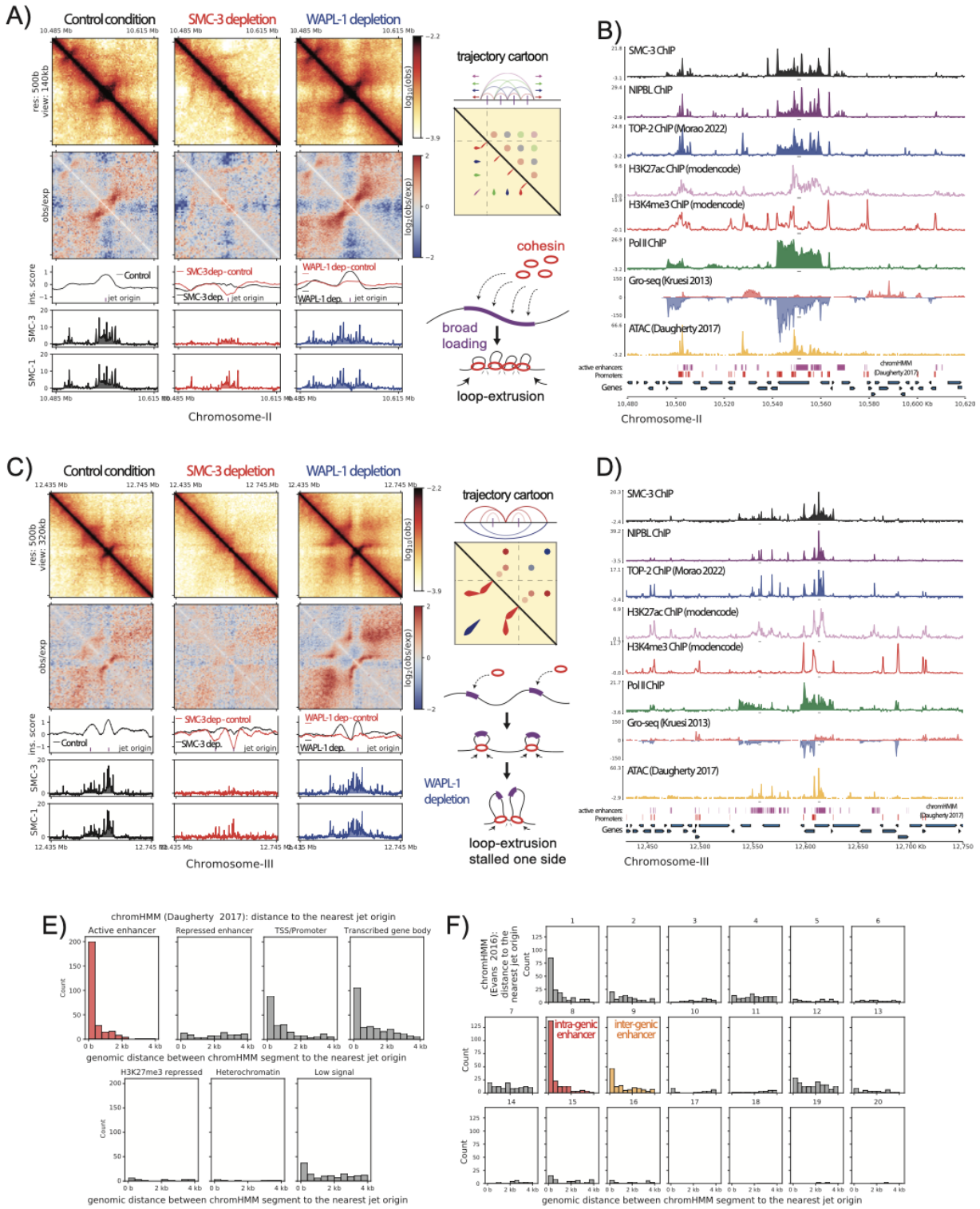

Figure 4. Loading site distribution effects on jet patterns.
A) Hi-C snapshot of a locus containing broadly distributed cohesin. Cartoon showing highly clustered loading events leading to cohesin-cohesin collisions, leading to domain-like patterns. B) Signal tracks and annotation for the region shown in panel A. SMC-3 (black), NIPBL (purple), TOP-2 (blue), H3K27ac (pink), H3K4me3 (red), and RNA Pol II (green) ChIP-seq tracks for control conditions are shown. Below are GRO-seq(46) and ATAC-seq (51) tracks and the annotated enhancer and promoter regions of chromHMM (51). C) Hi-C snapshot of a locus containing two separated and closely located cohesin domains. Cartoons showing the jet trajectory of two cohesin looping events leads to collision, which in turn leads to stalled one-sided loop extrusion and formation of secondary enriched contacts away from the main diagonal (blue trajectory in the cartoon). C) Signal tracks and annotation for the region shown in panel C. D) Histogram of 1kb binned genomic distance between identified jet origin in this paper and the annotated regions of chromHMM in (51). E) Histogram of 1kb binned genomic distance between identified jet origin in this paper and the annotated regions of chromHMM in (52). Abbreviated annotation from the original paper: 1-Promoter, 2-7 transcription elongation body, 8-intronic enhancer, 9-intergenic enhancer, 10-weak enhancer, 11-border, 12-20-low expression and/or repeats.

One hour depletion of SMC-3 or WAPL does not lead to changes in RNA Pol II binding

We used RNA Pol II ChIP-seq analyses to analyze the effect of reduced cohesin in SMC-3 depletion and ectopic cohesin binding upon WAPL knockdown. Unlike the striking changes observed in Hi-C, cohesin and WAPL depletion did not result in significant change in RNA Pol II binding (Figure 5B). To analyze the effect genome-wide, we categorized genes as being highly bound by cohesin in control compared to WAPL depletion (cohesin^{high} in control) or vice versa (cohesin^{high} in WAPL depletion). Consistent with increased spreading of cohesin in WAPL depletion, genes designated as cohesin^{high} in control condition were closer to jet origins compared to those designated cohesin^{high} in WAPL depletion (Figure 5C).

Analysis of cohesin binding across all jet origins by SMC-3 ChIP-seq reaffirms that cohesin binding reduces at the jet origin while increasing outwards upon WAPL knockdown (Figure 5D left panel). Accordingly, SMC-3 ChIP-seq signal across the transcription start and end sites of genes bound highly by cohesin in control and WAPL depletion conditions decreased and increased, respectively (Figure 5D right panel). RNA Pol II did not follow the pattern of cohesin. RNA Pol II ChIP-seq signal did not change upon SMC-3 or WAPL depletion across the jet origins and was not different for the two categories of genes in either condition (Figure 5E). These results indicate that acute depletion of cohesin and WAPL immediately change the 3D DNA contacts measured by Hi-C but do not result in detectable changes in RNA Pol II binding.

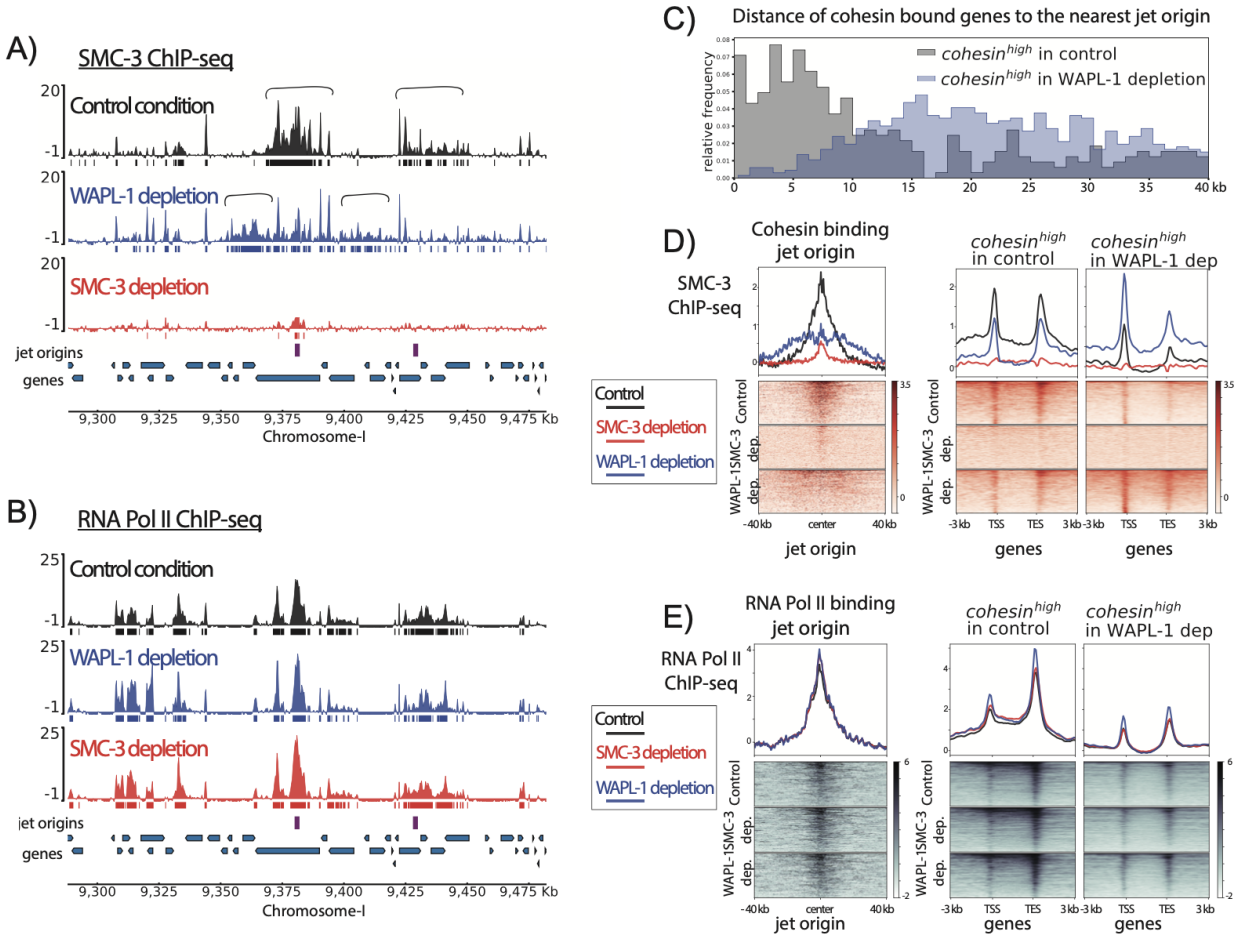

Figure 5 Acute depletion of cohesin and WAPL does not change RNA Pol II binding
A) SMC-3 ChIP-seq track for the control, WAPl-1, and SMC-3 depletion conditions at an example region. Brackets approximate regions containing cohesin^{high} genes in control top and cohesin^{high} genes in WAPL depletion conditions. B) RNA Pol II ChIP-seq tracks for the same conditions and region as panel A. C) Genes are categorized as cohesin^{high} in control (black) or in WAPL depletion (blue) if the gene contains MACS2 determined SMC-3 binding site in the control condition but not in WAPL depletion condition, and vice versa. C) The genomic distance between the genes and the nearest jet origins are calculated and plotted as 1kb-binned histogram. D) Shown are metaplots of SMC-3 ChIP-seq data centered at the jet origins (left panel) and the two categories of genes (right panel). E) Same as panel B but for RNA Pol II ChIP-seq data.

Cohesin depletion does not affect NIPBL binding

NIPBL orthologs were identified as a loading factor with its interacting partner SCC-4 in several species including *C. elegans* (29, 53). NIPBL was also proposed to be a processivity factor that travels with cohesin in the mammalian systems (4, 42, 43, 54). If cohesin mediates NIPBL crosslinking to chromatin, a portion of NIPBL sites must be SMC-3 dependent. This prediction was not met. Unlike SMC-1, NIBPL binding did not change upon SMC-3 depletion (Figure 6A).

Similarly, SMC-1 ChIP-seq signal was reduced and narrowed across the jet origins, but NIBPL signal did not alter (Figure 6B). Furthermore, upon SMC-3 depletion, persisting SMC-1 ChIP-seq peaks were closer to the jet origin, but NIPBL peaks position did not change (Figure 6C). Thus, NIPBL binding is not cohesin dependent in *C. elegans*.

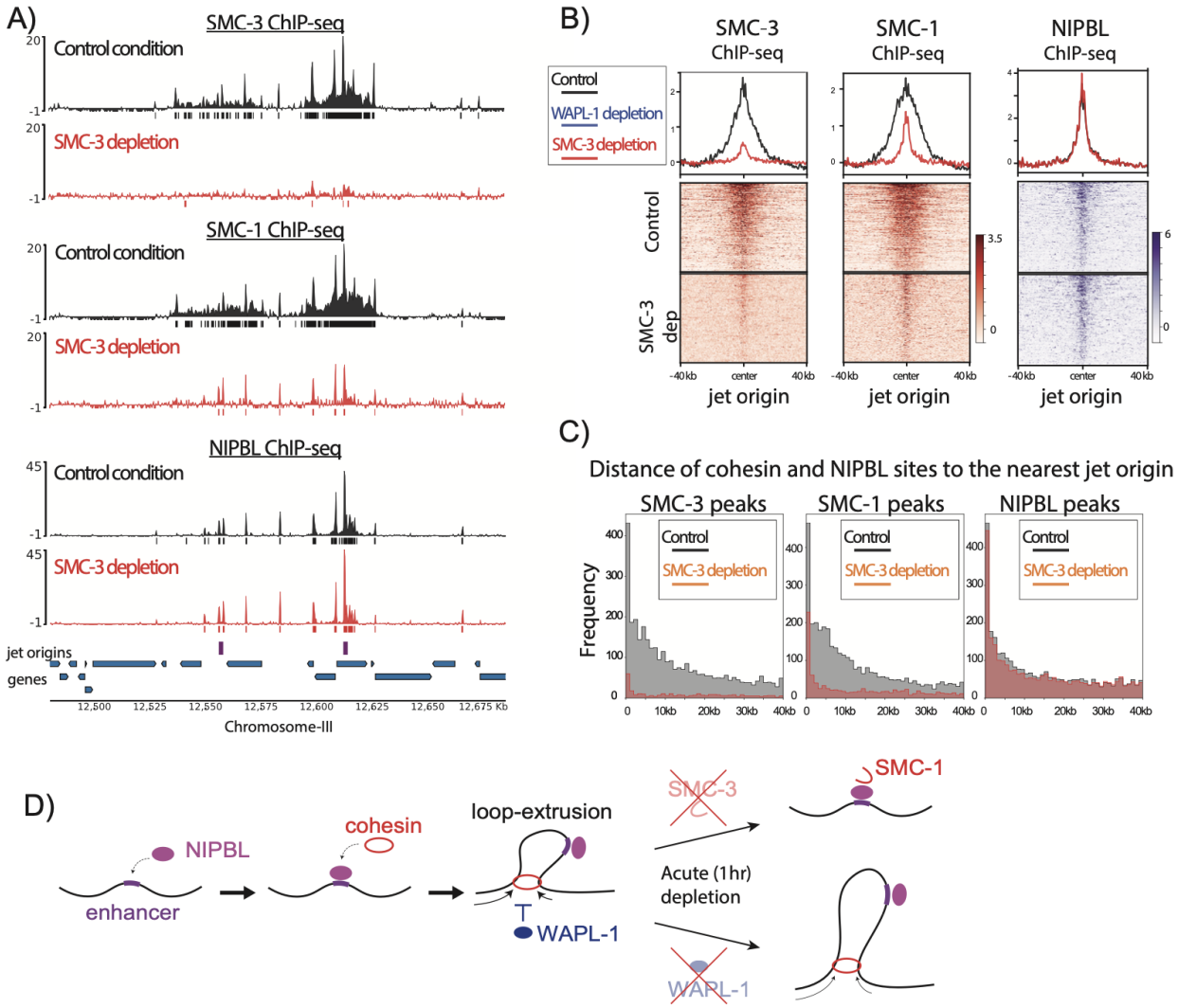

Figure 6 NIPBL does not spread with cohesin and is binding is independent of cohesin
A) Genome browser view of SMC-3 (top panel), SMC-1 (middle panel), and NIPBL (bottom panel) ChIP-seq profiles in control (black) and SMC-3 depletion (red) conditions. B) Metaplots of SMC-3, SMC-1, and NIPBL ChIP-seq scores centered at the jet origins for control (black) and SMC-3 depletion (red) conditions. C) Histogram of distance between the nearest jet origins and the binding sites of SMC-3, SMC-1, and NIPBL, under control (gray) and SMC-3 depletion (red) conditions. D) The proposed model of cohesin loading and loop extrusion events inferred from the perturbation experiments. Activated enhancers are bound by NIPBL which increase the frequency of cohesin loading at these sites. After loading, cohesin extrudes DNA in an effectively two-sided manner. Note that despite being depicted as a singular ring, the data cannot distinguish how many cohesin complexes are at the base of the loop. Upon acute depletion of SMC-3, the binding of NIPBL is unaffected and residual

amount of SMC-1 is found at loading site. The extruded loop is abolished. Upon acute depletion of the negative regulator WAPL-1, cohesin further extrudes DNA in two-sided manner away from the jet origin.

Discussion

While TAD formation by cohesin and CTCF have been implicated in proper development and normal physiology in the mammalian system, many species, including yeast, worms, and plants, contain cohesin but lack CTCF (55, 56). Here, we use *C. elegans* as a model to address the question: what does interphase cohesin do in organisms without CTCF? Our approach was to apply the auxin-inducible degradation system to acutely deplete the cohesin ATPase subunit SMC-3 or its negative regulator WAPL-1 in somatic cells in *C. elegans* larvae. Our results are consistent with a model that preferential loading of cohesin at active enhancers form a conserved 3D genome feature termed chromatin jets (Figure 6D).

Chromatin jets are a conserved feature of 3D genome organization mediated by cohesin

Recent studies demonstrate the existence of jets (aka plumes or fountains) in model species of worms, zebrafish and mammals, suggesting that preferential loading of cohesin followed by bi-directional loop extrusion leads is conserved across species (5-9). Based on analysis of individual jet examples and their genomic context, we further propose that chromatin jets reflect the frequency and distribution of cohesin loading, which correlates with the strength and distribution of cohesin loader NIPBL binding sites.

*NIPBL recruitment to a*ctive *enhancers may facilitate cohesin loading that form chromatin jets*

NIPBL (PQN-85/SCC-2) is required for cohesin binding to chromosomes across different species including *C. elegans* (29, 44, 53). We observed that the origin, pattern and trajectory of chromatin jets correlate with NIPBL binding, which does not require cohesin. Thus, we propose that the conserved function of NIPBL in *C. elegans* is to load cohesin. In many organisms, including *C. elegans* NIPBL binds to active enhancers and promoters (57-59). Analysis of cohesin binding in mammalian cells suggested that cohesin may be loaded at enhancers (39, 60). In a recent preprint using zebrafish, chromatin-jets correlated with enhancer activity across development and knockdown of pioneer transcription factors eliminated enhancer activity and chromatin jets originating at these sites (5). It is possible that transcription factors recruit NIPBL to mediate cohesin loading at active enhancers.

Clash of loop extruding cohesins creating a barrier effect

Modeling approaches are used to connect the behavior of single cohesin molecules to the population average data produced in Hi-C and we have interpreted our data in light of these studies (47). Our results suggest that frequent loading results in the clash of loop extruding cohesin molecules when these molecules are not removed from the DNA template by WAPL (Figure 4C). The resulting structure suggests cohesin continues to loop extrude on one side, while being stalled on the other. Therefore, an asymmetry in the loop extrusion is introduced by a barrier, in this case an incoming cohesin. Such a feature was also used in modeling to explain the flared structure of the jets, rather than a hairpin structure observed for bacterial SMCs (5, 61).

Clashing of incoming loop extruders may be a general feature of SMC complexes. In *C. elegans*, a specialized condensin I complex is loaded at distinct cis-regulatory elements on the X chromosomes for dosage compensation (DC). These sites also act to block loop extrusion by condensin DC (average loop size ~150 kb), forming TAD boundaries (38, 62). It is possible that frequent loading of condensin DC at these sites completely blocks the incoming molecules, because condensin loop extrude in one direction (38). In the case of cohesin, the clash of two cohesin molecules stops loop extrusion on the meeting side, but not the other. This supports the idea that unlike condensin, cohesin extrudes DNA in both directions *in vivo*.

RNA Polymerase II: barrier or facilitator of cohesin loop extrusion?

Earlier studies in yeast suggested that RNA Pol II may push cohesin (63, 64). More recent work used the framework of loop extrusion model and proposed that RNA Pol II and MCM complexes may be barriers to cohesin mediated loop extrusion (43, 65). It is possible that these specific proteins or their downstream effects, such as DNA topology regulate loop extrusion. Indeed *C. elegans* condensin DC requires topoisomerase II for its long-range processivity (30). We noticed that the asymmetry of our example jet in Figure 3 stems from stronger cohesin loop extrusion to the left side, where there is a long gene that is highly transcribed (Figure 3A). Here, it is possible that RNA Pol II facilitates cohesin loop extrusion, following those observations in yeast.

Chromatin jets and gene regulation

One hour depletion of cohesin and WAPL resulted in striking changes in the chromatin jets, but not on RNA Pol II binding measured by ChIP-seq (Figure 5). In the mammalian system, knockdown of cohesin also resulted in subtle changes in gene expression, yet mutations that reduce cohesin dosage or TAD boundaries produce significant changes (66, 67). It is possible that cohesin acts as a fine-tuner of transcription or function earlier in development, and once an epigenetic state is established, short-term depletion of cohesin does not result in changes in transcription (68).

A recent preprint reported TEV cleavage of two cohesin kleisin subunits over a period of ~24 hours from L1 larvae to L3 in *C. elegans* (69). A subsequent preprint detected fountains using average Hi-C plots and showed that the cleavage of COH-1 but not SCC-1 eliminated fountains (7). Authors also analyzed RNA-seq expression upon cohesin cleavage and reported a subtle reduction in the expression of genes close to enhancers near chromatin jets (7). This result agrees with a model that cohesin loading and extrusion loop out active enhancers and reduce their interaction with nearby promoters.

Evolution of cohesin activity

The co-evolution of underlying linear genome complexity and cohesin function may explain CTCF being lost in *C. elegans*. In the mammalian system, the relatively large cohesin loops are constrained by positioning of CTCF to prevent ectopic activation of promoters (70, 71). *C. elegans* cohesin makes ~10 fold smaller loops compared to the mammalian systems, which seems to scale with gene density (~one gene per 5 versus 100 kb). Whether cohesin mediated DNA loops reduce *cis*-element search space (72), or functions to cyclically accumulate factors for promoter activation (73), the relatively weak cohesin of *C. elegans* fits its underlying

compact genome, where enhancers are intragenic or immediately upstream of promoter (74). The presence of chromatin jets in *C. elegans* argues that preferential loading of cohesin at active enhancers is a conserved mechanism of 3D genome regulation. Within the context of a compact animal genome, how cohesin functions to regulate enhancers to accomplish cell-type specific gene expression is an intriguing question for future studies.

Acknowledgements:
JK and SE, and research in this manuscript were supported by NIGMS of the National Institutes of Health under award number R35 GM130311. Jun Kim was partially supported by NIGMS Predoctoral Fellowship T32HD007520. We thank Gencore at the NYU Center for Genomics and Systems Biology for sequencing and raw data processing.

Author Contributions:
JK and SE conceptualized the project and designed experiments. JK performed experiments and data analysis. JK and SE prepared figures and wrote the manuscript.

Declaration of interests:
None

References

1. J. A. da Costa-Nunes, D. Noordermeer, TADs: Dynamic structures to create stable regulatory functions. *Curr Opin Struct Biol* **81**, 102622 (2023).
2. G. Fudenberg, N. Abdennur, M. Imakaev, A. Goloborodko, L. A. Mirny, Emerging Evidence of Chromosome Folding by Loop Extrusion. *Cold Spring Harb Symp Quant Biol* **82**, 45-55 (2017).
3. I. F. Davidson *et al.*, CTCF is a DNA-tension-dependent barrier to cohesin-mediated loop extrusion. *Nature* **616**, 822-827 (2023).
4. Y. Kim, Z. Shi, H. Zhang, I. J. Finkelstein, H. Yu, Human cohesin compacts DNA by loop extrusion. *Science* **366**, 1345-1349 (2019).
5. A. Galitsyna *et al.*, Extrusion fountains are hallmarks of chromosome organization emerging upon zygotic genome activation. *bioRxiv* 10.1101/2023.07.15.549120, 2023.2007.2015.549120 (2023).
6. Y. Guo *et al.*, Chromatin jets define the properties of cohesin-driven in vivo loop extrusion. *Mol Cell* **82**, 3769-3780 e3765 (2022).
7. B. N. Isiaka *et al.*, Cohesin forms fountains at active enhancers in C. elegans. *bioRxiv* 10.1101/2023.07.14.549011, 2023.2007.2014.549011 (2023).
8. N. Q. Liu *et al.*, Rapid depletion of CTCF and cohesin proteins reveals dynamic features of chromosome architecture. *bioRxiv* 10.1101/2021.08.27.457977, 2021.2008.2027.457977 (2021).
9. C. L. Wike *et al.*, Chromatin architecture transitions from zebrafish sperm through early embryogenesis. *Genome Res* **31**, 981-994 (2021).
10. P. Heger, B. Marin, E. Schierenberg, Loss of the insulator protein CTCF during nematode evolution. *BMC Mol Biol* **10**, 84 (2009).

11. M. Hassler, I. A. Shaltiel, C. H. Haering, Towards a Unified Model of SMC Complex Function. *Curr Biol* **28**, R1266-R1281 (2018).
12. A. Cuadrado, A. Losada, Specialized functions of cohesins STAG1 and STAG2 in 3D genome architecture. *Curr Opin Genet Dev* **61**, 9-16 (2020).
13. A. F. Severson, L. Ling, V. van Zuylen, B. J. Meyer, The axial element protein HTP-3 promotes cohesin loading and meiotic axis assembly in C. elegans to implement the meiotic program of chromosome segregation. *Genes Dev* **23**, 1763-1778 (2009).
14. A. J. Wood, A. F. Severson, B. J. Meyer, Condensin and cohesin complexity: the expanding repertoire of functions. *Nat Rev Genet* **11**, 391-404 (2010).
15. M. R. Hernandez, M. B. Davis, J. Jiang, E. A. Brouhard, A. F. Severson, G. Csankovszki, Condensin I protects meiotic cohesin from WAPL-1 mediated removal. *PLoS Genet* **14**, e1007382 (2018).
16. Y. Mito, A. Sugimoto, M. Yamamoto, Distinct developmental function of two Caenorhabditis elegans homologs of the cohesin subunit Scc1/Rad21. *Mol Biol Cell* **14**, 2399-2409 (2003).
17. A. F. Severson, B. J. Meyer, Divergent kleisin subunits of cohesin specify mechanisms to tether and release meiotic chromosomes. *Elife* **3**, e03467 (2014).
18. Z. Yu, H. J. Kim, A. F. Dernburg, ATM signaling modulates cohesin behavior in meiotic prophase and proliferating cells. *Nat Struct Mol Biol* **30**, 436-450 (2023).
19. B. Langmead, S. L. Salzberg, Fast gapped-read alignment with Bowtie 2. *Nat Methods* **9**, 357-359 (2012).
20. P. Danecek *et al.*, Twelve years of SAMtools and BCFtools. *Gigascience* **10** (2021).
21. R. H. Ramirez-Gonzalez, R. Bonnal, M. Caccamo, D. Maclean, Bio-samtools: Ruby bindings for SAMtools, a library for accessing BAM files containing high-throughput sequence alignments. *Source Code Biol Med* **7**, 6 (2012).
22. H. M. Amemiya, A. Kundaje, A. P. Boyle, The ENCODE Blacklist: Identification of Problematic Regions of the Genome. *Sci Rep* **9**, 9354 (2019).
23. N. C. Durand *et al.*, Juicer Provides a One-Click System for Analyzing Loop-Resolution Hi-C Experiments. *Cell Syst* **3**, 95-98 (2016).
24. F. Ramirez *et al.*, High-resolution TADs reveal DNA sequences underlying genome organization in flies. *Nat Commun* **9**, 189 (2018).
25. J. Wolff *et al.*, Galaxy HiCExplorer: a web server for reproducible Hi-C data analysis, quality control and visualization. *Nucleic Acids Res* **46**, W11-W16 (2018).
26. N. Abdennur, L. A. Mirny, Cooler: scalable storage for Hi-C data and other genomically labeled arrays. *Bioinformatics* **36**, 311-316 (2020).
27. R. Gandhi, P. J. Gillespie, T. Hirano, Human Wapl is a cohesin-binding protein that promotes sister-chromatid resolution in mitotic prophase. *Curr Biol* **16**, 2406-2417 (2006).
28. S. Kueng *et al.*, Wapl controls the dynamic association of cohesin with chromatin. *Cell* **127**, 955-967 (2006).
29. J. Lightfoot, S. Testori, C. Barroso, E. Martinez-Perez, Loading of meiotic cohesin by SCC-2 is required for early processing of DSBs and for the DNA damage checkpoint. *Curr Biol* **21**, 1421-1430 (2011).
30. A. K. Morao, J. Kim, D. Obaji, S. Sun, S. Ercan, Topoisomerases I and II facilitate condensin DC translocation to organize and repress X chromosomes in C. elegans. *Mol Cell* **82**, 4202-4217 e4205 (2022).

31. L. Zhang, J. D. Ward, Z. Cheng, A. F. Dernburg, The auxin-inducible degradation (AID) system enables versatile conditional protein depletion in C. elegans. *Development* **142**, 4374-4384 (2015).
32. J. E. Sulston, H. R. Horvitz, Post-embryonic cell lineages of the nematode, Caenorhabditis elegans. *Dev Biol* **56**, 110-156 (1977).
33. H. B. Brandao, P. Paul, A. A. van den Berg, D. Z. Rudner, X. Wang, L. A. Mirny, RNA polymerases as moving barriers to condensin loop extrusion. *Proc Natl Acad Sci U S A* **116**, 20489-20499 (2019).
34. N. L. Sullivan, K. A. Marquis, D. Z. Rudner, Recruitment of SMC by ParB-parS organizes the origin region and promotes efficient chromosome segregation. *Cell* **137**, 697-707 (2009).
35. X. Wang, H. B. Brandao, T. B. Le, M. T. Laub, D. Z. Rudner, Bacillus subtilis SMC complexes juxtapose chromosome arms as they travel from origin to terminus. *Science* **355**, 524-527 (2017).
36. X. Wang *et al.*, In Vivo Evidence for ATPase-Dependent DNA Translocation by the Bacillus subtilis SMC Condensin Complex. *Mol Cell* **71**, 841-847 e845 (2018).
37. S. E. Albritton, A. L. Kranz, L. H. Winterkorn, L. A. Street, S. Ercan, Cooperation between a hierarchical set of recruitment sites targets the X chromosome for dosage compensation. *Elife* **6** (2017).
38. J. Kim *et al.*, Condensin DC loads and spreads from recruitment sites to create loop-anchored TADs in C. elegans. *Elife* **11** (2022).
39. R. Han *et al.*, Targeted cohesin loading characterizes the entry and exit sites of loop extrusion trajectories. *bioRxiv* 10.1101/2023.01.04.522689, 2023.2001.2004.522689 (2023).
40. K. P. Hopfner, J. A. Tainer, Rad50/SMC proteins and ABC transporters: unifying concepts from high-resolution structures. *Curr Opin Struct Biol* **13**, 249-255 (2003).
41. K. W. Muir, Y. Li, F. Weis, D. Panne, The structure of the cohesin ATPase elucidates the mechanism of SMC-kleisin ring opening. *Nat Struct Mol Biol* **27**, 233-239 (2020).
42. D. Alonso-Gil, A. Cuadrado, D. Gimenez-Llorente, M. Rodriguez-Corsino, A. Losada, Different NIPBL requirements of cohesin-STAG1 and cohesin-STAG2. *Nat Commun* **14**, 1326 (2023).
43. E. J. Banigan *et al.*, Transcription shapes 3D chromatin organization by interacting with loop extrusion. *Proc Natl Acad Sci U S A* **120**, e2210480120 (2023).
44. R. Ciosk *et al.*, Cohesin's binding to chromosomes depends on a separate complex consisting of Scc2 and Scc4 proteins. *Mol Cell* **5**, 243-254 (2000).
45. M. H. Kagey *et al.*, Mediator and cohesin connect gene expression and chromatin architecture. *Nature* **467**, 430-435 (2010).
46. W. S. Kruesi, L. J. Core, C. T. Waters, J. T. Lis, B. J. Meyer, Condensin controls recruitment of RNA polymerase II to achieve nematode X-chromosome dosage compensation. *Elife* **2**, e00808 (2013).
47. E. J. Banigan, A. A. van den Berg, H. B. Brandao, J. F. Marko, L. A. Mirny, Chromosome organization by one-sided and two-sided loop extrusion. *Elife* **9** (2020).
48. C. Arnould *et al.*, Loop extrusion as a mechanism for formation of DNA damage repair foci. *Nature* **590**, 660-665 (2021).
49. J. Gassler *et al.*, A mechanism of cohesin-dependent loop extrusion organizes zygotic genome architecture. *EMBO J* **36**, 3600-3618 (2017).

50. K. E. Polovnikov, B. Slavov, S. Belan, M. Imakaev, H. B. Brandão, L. A. Mirny, Fractal polymer with loops recapitulates key features of chromosome organization. *bioRxiv* 10.1101/2022.02.01.478588, 2022.2002.2001.478588 (2023).
51. A. C. Daugherty, R. W. Yeo, J. D. Buenrostro, W. J. Greenleaf, A. Kundaje, A. Brunet, Chromatin accessibility dynamics reveal novel functional enhancers in C. elegans. *Genome Res* **27**, 2096-2107 (2017).
52. K. J. Evans, N. Huang, P. Stempor, M. A. Chesney, T. A. Down, J. Ahringer, Stable Caenorhabditis elegans chromatin domains separate broadly expressed and developmentally regulated genes. *Proc Natl Acad Sci U S A* **113**, E7020-E7029 (2016).
53. V. C. Seitan *et al.*, Metazoan Scc4 homologs link sister chromatid cohesion to cell and axon migration guidance. *PLoS Biol* **4**, e242 (2006).
54. I. F. Davidson, B. Bauer, D. Goetz, W. Tang, G. Wutz, J. M. Peters, DNA loop extrusion by human cohesin. *Science* **366**, 1338-1345 (2019).
55. P. Dong *et al.*, 3D Chromatin Architecture of Large Plant Genomes Determined by Local A/B Compartments. *Mol Plant* **10**, 1497-1509 (2017).
56. P. Heger, B. Marin, M. Bartkuhn, E. Schierenberg, T. Wiehe, The chromatin insulator CTCF and the emergence of metazoan diversity. *Proc Natl Acad Sci U S A* **109**, 17507-17512 (2012).
57. G. A. Busslinger *et al.*, Cohesin is positioned in mammalian genomes by transcription, CTCF and Wapl. *Nature* **544**, 503-507 (2017).
58. A. L. Kranz, C. Y. Jiao, L. H. Winterkorn, S. E. Albritton, M. Kramer, S. Ercan, Genome-wide analysis of condensin binding in Caenorhabditis elegans. *Genome Biol* **14**, R112 (2013).
59. Y. Zhu, M. Denholtz, H. Lu, C. Murre, Calcium signaling instructs NIPBL recruitment at active enhancers and promoters via distinct mechanisms to reconstruct genome compartmentalization. *Genes Dev* **35**, 65-81 (2021).
60. E. S. M. Vos *et al.*, Interplay between CTCF boundaries and a super enhancer controls cohesin extrusion trajectories and gene expression. *Mol Cell* **81**, 3082-3095 e3086 (2021).
61. H. B. Brandao, Z. Ren, X. Karaboja, L. A. Mirny, X. Wang, DNA-loop-extruding SMC complexes can traverse one another in vivo. *Nat Struct Mol Biol* **28**, 642-651 (2021).
62. E. C. Anderson *et al.*, X Chromosome Domain Architecture Regulates Caenorhabditis elegans Lifespan but Not Dosage Compensation. *Dev Cell* **51**, 192-207 e196 (2019).
63. E. F. Glynn *et al.*, Genome-wide mapping of the cohesin complex in the yeast Saccharomyces cerevisiae. *PLoS Biol* **2**, E259 (2004).
64. A. Lengronne *et al.*, Cohesin relocation from sites of chromosomal loading to places of convergent transcription. *Nature* **430**, 573-578 (2004).
65. B. J. H. Dequeker *et al.*, MCM complexes are barriers that restrict cohesin-mediated loop extrusion. *Nature* **606**, 197-203 (2022).
66. C. T. Cummings, M. J. Rowley, Implications of Dosage Deficiencies in CTCF and Cohesin on Genome Organization, Gene Expression, and Human Neurodevelopment. *Genes (Basel)* **13** (2022).
67. A. Hafner, A. Boettiger, The spatial organization of transcriptional control. *Nat Rev Genet* **24**, 53-68 (2023).
68. B. Pelham-Webb, D. Murphy, E. Apostolou, Dynamic 3D Chromatin Reorganization during Establishment and Maintenance of Pluripotency. *Stem Cell Reports* **15**, 1176-1195

(2020).
69. M. Das *et al.*, Condensin I folds the C. elegans genome. *bioRxiv* 10.1101/2022.06.14.495661, 2022.2006.2014.495661 (2022).
70. D. Hnisz, D. S. Day, R. A. Young, Insulated Neighborhoods: Structural and Functional Units of Mammalian Gene Control. *Cell* **167**, 1188-1200 (2016).
71. M. Levine, C. Cattoglio, R. Tjian, Looping back to leap forward: transcription enters a new era. *Cell* **157**, 13-25 (2014).
72. T. S. Hsieh, C. Cattoglio, E. Slobodyanyuk, A. S. Hansen, X. Darzacq, R. Tjian, Enhancer-promoter interactions and transcription are largely maintained upon acute loss of CTCF, cohesin, WAPL or YY1. *Nat Genet* **54**, 1919-1932 (2022).
73. J. Y. Xiao, A. Hafner, A. N. Boettiger, How subtle changes in 3D structure can create large changes in transcription. *Elife* **10** (2021).
74. V. Reinke, M. Krause, P. Okkema, Transcriptional regulation of gene expression in C. elegans. *WormBook* 10.1895/wormbook.1.45.2, 1-34 (2013).